Zirconia Pillared Clays: Synthesis, Characterization and Catalytic Properties in the NO_x Selective Reduction by Hydrocarbons in the Oxygen Excess

V. A. SADYKOV[1,2], T. G. KUZNETSOVA[1], V. P. DORONIN[1], T. P. SOROKINA[1], G. M. ALIKINA[1], D. I. KOCHUBEI[1], B. N. NOVGORODOV[1], E. A. PAUKSHTIS[1], V. B. FENELONOV[1], V. I. ZAIKOVSKII[1], V. A. ROGOV[1], V. F. ANUFRIENKO[1], N. T. VASENIN[1], V. A. MATYSHAK[3], G. A. KONIN[3], A. Ya. ROZOVSKII[4], V. F. TRETYAKOV[4], T. N. BURDEYNAYA[4], J. R. H. ROSS[5] and J. P. BREEN[5]

[1]*G. K. Boreskov Institute of Catalysis, Siberian Branch of the Russian Academy of Sciences, Pr. Akademika Lavrentyeva 5, Novosibirsk 630090 (Russia)*

E-mail: sadykov@catalysis.nsk.su

[2]*Novosibirsk State University, Ul. Pirogova 2, Novosibirsk 630090 (Russia)*

[3]*N. N. Semenov Institute of Chemical Physics, Russian Academy of Sciences, Ul. Kosygina 4, Moscow 117977 (Russia)*

[4]*A. V. Topchiev Institute of Petrochemical Synthesis, Russian Academy of Sciences, Leninskiy pr. 29, Moscow 117912 (Russia)*

[5]*University of Limerick, Technology Park, Limerick (Ireland)*

Abstract

Procedures for synthesis of thermally stable up to 750 °C zirconia-pillared clays (ZrPC) *via* intercalation of a montmorillonite clay with zirconium polyoxocations modified by cations of Ce, Fe, Al, Ca, Sr, Ba, were elaborated. Optimization of the preparation procedure allowed to obtain samples with specific surface area up to 300–400 m^2/g, the gallery height up to 10 Å and micropore volume up to 0.13 m^2/g. Active components comprised of copper cations and/or Pt clusters were supported on ZrPC by using photoassisted deposition. The structural and surface properties of pillars and effects of mutual interaction between the nanosized zirconia particles, and metal and oxide components were elucidated by using EXAFS, UV-Vis, ESR, H_2 TPR, NO_x TPD and FTIRS of adsorbed CO molecules. Catalytic properties of these systems were characterized in the reactions of NO_x selective reduction in the excess of oxygen by propane, propylene and decane. Strong interaction between the Pt atoms and copper cations resulted in substantial variation of the reactivity of the surface oxygen as well as bonding strength and coverages of surface ad-NO_x species. It was reflected in substantial improvement of the low-temperature activity of these systems as compared with those containing separate components. The nature of cation used for pillar modification was found to affect catalytic properties of supported active components, which can be explained by variation of the pillars structure and uniformity of their spatial distribution in clay galleries.

INTRODUCTION

Selective catalytic reduction of nitrogen oxides by hydrocarbons in the excess of oxygen (NO_x HC SCR) is now considered as one of the promising ways for NO_x abatement from exhausts of lean – burn and Diesel engines. Systems based upon platinum metal or transition metal cations supported onto zeolites, alumina and zirconia were shown to be quite efficient in this process [1]. In the low-temperature range and at high space velocities, the highest performance is observed for catalysts containing precious metals. However, they are characterized by rather narrow operation temperature window, and generate a lot of nitrous oxide in the process. At temperatures close to real temperatures of automotive exhausts (400–700 °C), the most active and selective are copper-containing systems, such as those based

upon Cu-ZSM-5 [2]. However, they have some drawbacks restricting their practical applications, first of all, irreversible deactivation in real humid feeds due to dealumination. Systems based upon pillared clays (PCs) with the pore structure formed by galleries between the alumosilicate layers with typical sizes in the range of supermicropores (8–25 Å) appear to be promising for NO_x SCR [3]. These materials are obtained via cation exchange of large inorganic polynuclear hydroxocationic species of Fe, Zr, Cr, Ti (either pure or modified with another cations) into the clay interlayer positions. Subsequent thermal treatment rearranges the structure of polycations into that of oxidic nanoparticles (pillars) propping the alumosilicate layers [4]. PCs possess well-developed pore structure and good thermal and hydrothermal stability. However, up to now, no systematic studies of catalytic properties of those materials in the NO_x HC SCR have been undertaken.

In previous publications [5–7], procedures for pillaring of natural montmorillonite clays of Kazakhstan deposits with zirconia polycations including those modified by cerium and alkaline-earth cations were described. Some properties of pillaring species in solution and pillared clays were presented. The structure of pillaring species [6] was shown to be based upon several stacked Zr tetramers being mainly preserved in calcined pillared clays, their size and structure being affected by modifying cations. Preliminary results for Cu- or Co-loaded Zr- or Ce + Zr-PC [5, 7] revealed a lower activity of those catalysts in the NO_x HC SCR as compared with the same active components supported on bulk partially stabilized zirconia or alumina carriers [9, 10] or ZSM-5 zeolites [11]. Rather low rates of HC oxidation revealed for PC-based catalysts suggest that their poor performance in NO_x SCR is due to inability to efficiently activate hydrocarbons. Promotion of those systems with Pt could impart this function, since Pt is known for its ability to easily disrupt C–H bond. Variation of the nature of cation used for zirconia pillar modification might also affect the mode of supported transition metal cations interaction with pillars, and, hence, their catalytic properties in the reactions of interest.

Hence, the aim of this work was to synthesize a number of zirconia pillared clays with systematic variation of the nature and content of pillars stabilizing cations (Ca, Sr, Ba, Ce, Fe), to characterize their pore structure, to elucidate adsorption properties and reactivity of transition metal cations and Pt clusters on pillars as related to their catalytic activity in the NO_x selective reduction by propane, propylene and decane.

EXPERIMENTAL

Catalyst preparation

Synthesis of samples have been carried out according to procedures described in [5–7]. Zirconia- pillared clays (zirconia content 15–30 %) were synthesized using a Ca-montmorillonite clay (CaO content 2 % mass; Fe admixture content ~0.2 % mass). To synthesize pillaring macrocations, 0.1 M $ZrOCl_2$ $8H_2O$ solution (Ca, Sr, Ba, Ce, or Fe nitrates were added to modify the properties of zirconia pillars) aged at 60 °C for 16 h was used. Pillaring was carried out either at 60 °C for 16–20 h (for most samples), or at room temperature for 48 h, followed by samples washing with distilled water, drying and calcinations at 350–750 °C. Cu (1.4 % mass), Pt (0.3 % mass) and Pt (0.3 % mass) + Cu (1.4 % mass)-containing catalysts based upon montmorillonite clay pillared with partially stabilized ZrO_2 (15–30 % mass) were prepared through the photoassisted deposition of those components from water solutions of Cu acetate and H_2PtCl_6, separately or consecutively, respectively, followed by drying and calcination at 400 °C [8].

The chemical composition of samples was analyzed by the atomic absorption spectroscopy (a Karl Zeiss Jena AAS1N spectrometer). The X-ray phase analysis was carried out by using a HZG-4C diffractometer with monochromatized CuK_α radiation.

Adsorption characteristics were measured on a Micromeritics ASAP-2400 installation by N_2 adsorption at ~77 K. The micropore volume was estimated by using t-method [12] and Dubinin – Radushkevich method [13].

EXAFS spectra of the K-edge of Zr X-ray absorption were obtained at the EXAFS Sta-

tion of the Siberian Center of Synchrotron Radiation (Novosibirsk, Russia). The experimental procedure and data analysis by EXCURV-92 software are described in details in [8].

Samples particles morphologies were characterized using TEM (JEM 2010, 200 kV).

ESR spectra of Cu^{2+} in catalyst samples were obtained at 300 and 77 K on a JES-3BX spectrometer using calcined air-stored samples without any pretreatment before measurements.

UV-Vis spectra were recorded using a Shimadzu 8300 spectrometer equipped with a diffuse scattering DRS 8000 cell. Spectra were recorded in the 10 000–60 000 cm^{-1} range with 4 cm^{-1} resolution, the number of scans being equal to 50. Samples were loaded into the vacuum cells equipped with CaF windows. To decrease the mirror reflection, a sample layer was inclined for 20–25 % with respect to the horizontal plane.

Surface properties were probed by the Fourier Transform Infrared Spectroscopy (FTIRS) of adsorbed CO (IFS 113V Bruker spectrometer). In those experiments, samples were pressed in wafers with densities 4.4–22.7 mg/cm^2 and pretreated in the IR cell first at 100 Torr of O_2 then in vacuum at 400 °C for 1 h. CO was adsorbed at 77 K first by introducing several doses (each CO dose corresponds to ~4 μmol), finally setting CO pressure to 10 Torr. After cell evacuation at 77 K, sample was warmed up to room temperature, then CO was added to 10 Torr with subsequent evacuation. The spectra in the carbonyl and hydroxyl stretching ranges were recording at each step. By using a routine computer processing, the data were presented as absorbance normalized to the unit weight of sample, which allows one to directly compare results obtained for different samples [8].

The temperature-programmed desorption of NO_x (TPD) from the surface of samples after oxidative pretreatment (1 h, 400 °C, O_2 flow) was carried out with the temperature ramp from 25 to 550° at 10 °C/min rate using a chemiluminescence NO_x Beckman analyzer and following procedures described earlier in details [8]. For systems studied here subjected to the oxidative pretreatment, no evolution of nitrous oxide was detected in TPD runs, which was checked by using a Perkin Elmer Spectrum RX I FT-IR system and a gas cell.

In H_2 TPR experiments, 0.4 g of sample was loaded into a reactor and pretreated in a flow of oxygen at 400 °C for 1 h followed by cooling to room temperature in the oxygen then purging by Ar. Reduction of the sample was carried out from 40 to 650 °C in a flow of 10 % H_2/Ar (40 ml/min) at a heating rate of 10 °/min. The consumption of H_2 was monitored continuously by the thermal conductivity detector.

The properties of catalysts in the NO_x HC-SCR reactions were tested in flow microreactors using procedures described previously [9] using mainly mixtures with standard compositions 0.1 % C_3H_8 + 0.1 % NO + 1 % O_2 in He (feed 1, GHSV 12000/h), 0.2 % C_3H_6 + 0.2 % NO + 2.5 % O_2 in N_2 (feed 2, GHSV 18 000/h), 0.05 % $C_{10}H_{22}$ + 0.15 % NO in air (feed 3, GHSV 13000/h) and GC + chemiluminescence analysis of starting compounds and products. The error in determining NO_x conversions was found to be *ca.* 5 % rel.

RESULTS AND DISCUSSION

Pore structure and phase composition of samples

Table 1 lists compositions of ZrPC samples synthesized and studied within this research. The volume of micropores is in the range of the best values earlier reported for clays pillared with zirconia [14–17] or alumina [18, 19]. Around half of the integral pore volume is due to mesopores emerged due to defects in the clay sheets stacking. In no case X-ray detectable zirconia phase admixtures were observed. Pore structure withstands overheating up to 750 °C without collapse, which is comparable with the best results reported by Ohtsuka *et al.* [20]. Such a stability implies reasonably uniform spatial distribution of pillars within galleries [20]. This conclusion agrees with nearly periodic hexagonal-type arrangement of nanometer-size white and dark dots in the high-resolution ($\times 10^6$) images of ZrPC platelets (not shown for brevity). Any separate ZrO_2 particles or clay sheets exfoliation/bending were not observed.

TABLE 1

Some characteristics of ZrPC samples

Sample No.	Designation	Pillar content, % mass	Type and content (% mass) of modifying cation	ΣBET, m^2/g (calcined at T, °C)	d_{001}, Å, after calcinations at T, °C				Pore volume, cm^3/g[a]	
					100	350	500	750	Integral	Micro[b]
1	CB-72	20	Ca, 0.2	460(350); 265(500)	17.7	17.4	17.6		0.18	0.13
2	CB-73	20	Sr, 0.2	430(350); 240(500)	17.8	17.5			0.18	0.12
3	CB-74	20	Ba, 0.2	430(350); 230(500)		17.5	17.0		0.18	0.12
4	CB-87	20	Ce, 0.02	315(500)	20.0	18.8	18.5		0.2	0.12
5	CB-88	20	Ce, 0.06	310(500)	20.5		18.5		0.22	0.13
6	CB-89	20	Ce, 0.36	300(500)	21.0	19.0			0.15	0.11
7	CB-92	20	Fe, 0.6	315(350)						
8	CB-93	20	Fe, 0.8	370(350)		18.2				
9	CB-95	20	Fe, 0.6	360(350)						
10	CB-96	20	Fe, 1.1	350(350)						
11	CB-98[c]	20	Ce, 0.06	270(500)	17.7				0.16	0.09
12	CB-99[c]	16	Ce, 0.31	320(500)	Broadened peak				0.21	0.10
13	CB-100[c]	15	Fe, 1.0	310(500)					0.22	0.10
14	CB-101	31	–	260(500)		19.8	18.0	16.7		0.13
15	CB-102	20	Al, 4.0	240(500)						

[a]After calcinations at 500 °C.

[b]Results by D-R and t-method coincide.

[c]Room-temperature pillaring (see experimental part).

Structural features of pillars

Some EXAFS parameters for ZrPC samples are presented in Table 2. As compared with bulk mesoporous zirconia samples [8], Zr–Zr coordination number (CN) in pillars is decreased while that for Zr–O distance is increased. Comcomitantly, Zr–O distance in pillars is larger and that of Zr–Zr is smaller than in bulk analogs. These results indicate that the structure of zirconia pillars differs considerably with that of bulk dispersed zirconia samples. Low Zr–Zr coordination numbers for pillars are close to that in Zr_4 polynuclear pillaring species in solution [6, 21] indicating similarity of their structure. The highest coordination numbers are observed for pillars modified with Ce cations identical by charge and close by size to Zr cations. All other modifying cations strongly distort the pillar structure (Zr–Zr CN decreases), thus suggesting their incorporation into pillars. More disordered structure of Sr-containing zirconia pillars (lower Zr–Zr coordination numbers and shorter Zr–Zr distances as compared with those for Ca-containing samples) seems to correlate with more distorted structure and broad size/shape variation of Zr pillaring species in solutions containing Sr cation [6]. In the first approximation, variation of the modifying cation content caused no detectable effect on the pillar structure. Note that supporting copper cations on Ce-modified pillars distorts their structure as well, thus implying Cu incorporation into the bulk of nanosized pillars. Higher Zr–Zr CN for Cu/Ce-ZrPC as compared with that for Cu/ZrPC sample imply less strong interaction of Cu cations with pillars modified by Ce cations.

Properties of supported active components

UV-Vis. For samples with supported copper, absorption at ~12 500 cm^{-1} corresponding to *d-d* transition in Cu^{2+} cations with distorted octahedral coordination is observed (Fig. 1). The intensity of absorption increases with the copper content. A weak absorption in the range of 18 000–30 000 cm^{-1} differing by intensity from sample to sample is observed as well. This absorption is usually assigned to charge transfer bands in clustered copper oxidic species [22]. The intensity of this absorption varies markedly from sample to sample, being the lowest

TABLE 2

EXAFS parameters for Zr-containing samples

Sample	Sphere	Coordination number	Distance, Å	Debye–Waller factor $2\sigma^2$, $Å^2$
Ce-ZrPC CB-87, 88, 89 98, 99	Zr–O	2.4	2.10	0.006
	Zr–O	2.4`	2.23	0.006
	Zr–Zr	1.0	3.53	0.010
	Zr–Zr	1.3	3.53	0.014
Ca-ZrPC CB-72	Zr–O	4.6	2.15	0.017
	Zr–Zr	0.5	3.44	0.006
	Zr–Zr	0.5	3.56	0.012
Sr-ZrPC CB-74	Zr–O	4.7	2.13	0.016
	Zr–Zr	0.4	3.41	0.006
	Zr–Zr	0.4	3.53	0.011
Fe-ZrPC CB-92, 93, 95, 96, 100	Zr–O	2.4	2.10	0.006
	Zr–O	2.4	2.22	0.006
	Zr–Zr	1.0	3.54	0.011
Cu/Ce-ZrPC	Zr–O	5.1	2.14	0.017
	Zr–Zr	0.9	3.48	0.014
CaO-ZrO_2 bulk	Zr–O	2.7	2.09	0.008
	Zr–Zr	6.1	3.65	0.015
	Zr–Zr	~1.5	~5.2	

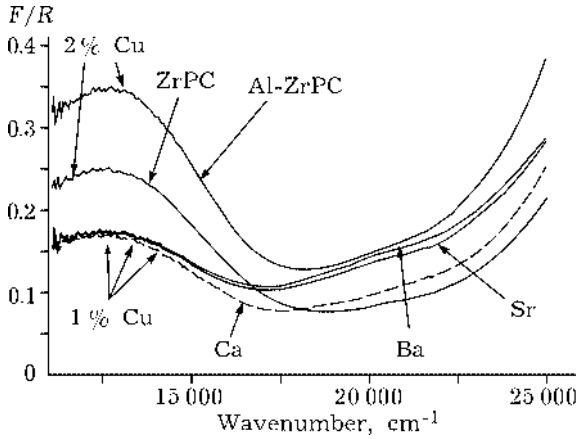

Fig. 1. UV-Vis spectra for ZrPC loaded with copper cations. Pillars are either pure zirconia or stabilized by Al, Ca, Sr and Ba cations.

for sample with the highest content of zirconia (see Fig. 1, curve *1*). Among samples with zirconia pillars stabilized by alkaline-earth cations, the intensity of that absorption is lowest for Ca-containing sample, implying a lower share of clustered oxidic species.

ESR. Typical ESR spectra of copper-containing samples are presented in Fig. 2. From a rather complex spectrum indicating existence of several paramagnetic centers, a signal with parameters $g_{\|} = 2.42$; $A_{\|} = 106$ Gs, $g_{\perp} = 2.05$ corresponding to isolated Cu^{2+} cations in distorted octahedral coordination [22–24] can be separated. These parameters are nearly identical for copper cations fixed at zirconia pillars stabilized by different cations, being also not affected by subsequent Pt deposition. In addition, a signal corresponding to magnetically

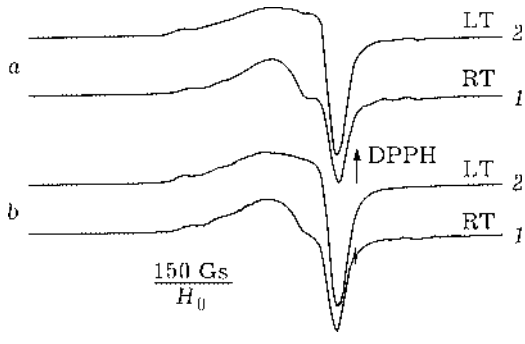

Fig. 2. Typical ESR spectra for 1.4 % mass Cu-containing (*a*) or 0.3 % Pt + 1.4 % mass Cu-containing (*b*) samples of pillared clays. Spectra recorded at room temperature (RT) or at liquid N_2 temperature (LT): *a* – PD-100, Ce-modified pillars; *b* – PD-114, Fe-modified pillars; *k* value: 4(*1*), 1 (*2*).

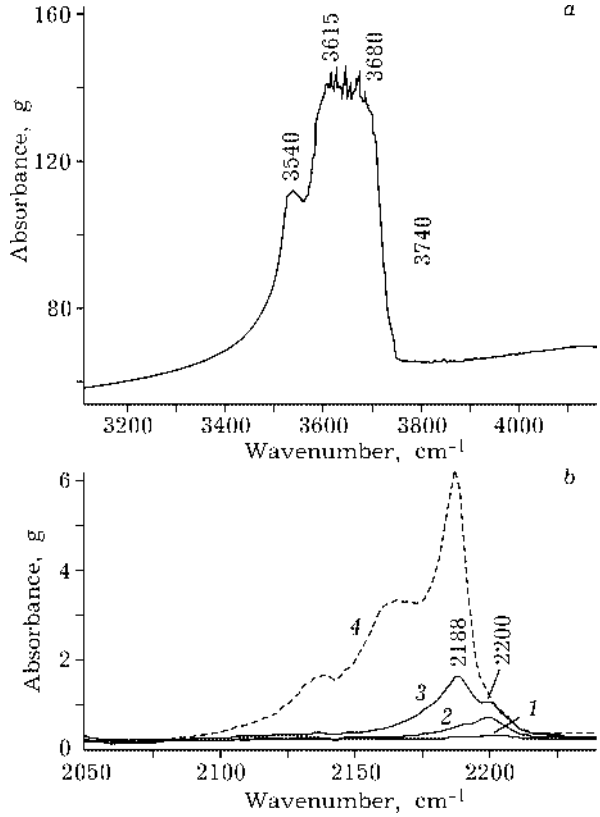

Fig. 3. FTIRS spectra of the initial montmorillonite clay in the hydroxyls stretching region (*a*) and spectra of CO adsorbed at the surface of the initial montmorillonite clay at 77 K (*b*). Spectra recorded after 1 dose of CO (*1*), 4 doses (*2*), 9 doses (*3*) and under 10 Torr CO (*4*).

coupled copper cations [22] is superimposed, though its intensity is low. In all cases, the integral intensity of the ESR spectrum corresponds to around 5 % of the copper cations present in a sample. Hence, predominant part of copper cations fixed at zirconia pillars exists as copper oxidic species and/or Cu^{+} cations not detected by ESR.

Surface properties by FTIRS. For the initial (before pillaring) clay (Fig. 3, *a*), intense bands of hydroxyl groups were observed at ~3540, 3615 and 3660 cm^{-1}. Those bands correspond to bridging hydroxyls bound with Si and Al cations at the surface of clay sheets [14]. A weak Lewis acid sites corresponding to coordinatively unsaturated Al^{3+} cations in tetrahedral coordination (band at ~2200 cm^{-1}, a minor part of centers with a higher strength) and octahedral coordination (band at ~2190 cm^{-1}, dominates at higher CO coverage) are revealed by FTIRS of CO adsorbed at 77 K (see Fig. 3, *b*).

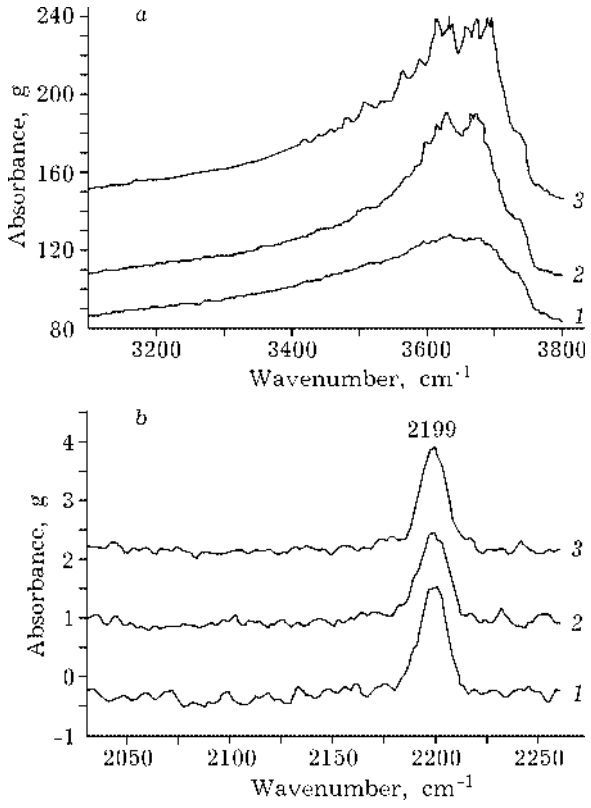

Fig. 4. Typical FTIRS spectra of ZrPC samples in the hydroxyls stretching region (*a*) and spectra of CO adsorbed at the surface of ZrPC samples at 77 K after the first dose of CO (*b*): *1* – Ca-ZrPC, *2* – Ba-ZrPC, *3* – Sr-ZrPC.

For zirconia-pillared clays, spectral characteristics of Broensted and Lewis acid sites differ with those for both the initial clay (vide supra) and bulk highly dispersed zirconia samples partially stabilized by alkaline-earth cations [8]. As a typical example, Fig. 4 illustrates FTIRS spectra of ZrPC stabilized by Ca, Sr or Ba cations in hydroxyls and CO stretching range. According to existing assignment [25–27], for bulk dispersed zirconia samples, the bands observed in the 3600–3800 cm^{-1} range correspond to hydroxyls located at the most developed zirconia faces of the (110) and (111) types, namely, to terminal OH groups (band ~3770 cm^{-1}) and bridging two-coordinated (~3730 cm^{-1}) and three-coordinated (~3670 cm^{-1}) hydroxyls. As can be deduced from Fig. 4, *a*, for ZrPC terminal hydroxyls are absent, while band positions correspond to strongly bound bridging hydroxyls. This agrees with the structure of nanosized pillars approaching that of a partially dehydrated Zr tetramer with connecting bridging hydroxyls between zirconium cations [6, 14, 21]. A predominant part of hydroxyls typical to the initial clay are removed. It can be assigned to neutralization of the negative charge of the alumosilicate layers by positively charged zirconium polycations instead of protons as takes place in the non-pillared clays. The most apparent suppression of the initial clay acidity is expressed for Ca-ZrPC, thus suggesting a more uniform distribution of pillars for this sample. The intensity of hydroxyl bands related to the surface unit of zirconia (*ca.* 50 m^2 ZrO_2/g of PC as estimated by using the pillar size ~10 Å and zirconia content), was found to be much higher as compared with their intensity for bulk mesoporous zirconia samples [8], thus evidencing a much higher degree of hydroxylation for nanosized zirconia pillars.

The nature and intensity of the most strong Lewis acid sites revealed by CO adsorption at 77 K (see Fig. 4, *b*) is greatly changed as compared with that for the initial clay (see Fig. 3, *b*). By the band position, these centers correspond to coordinatively unsaturated Zr^{4+} identical to those observed for bulk dispersed zirconia samples [8, 27]. The highest surface density of the Lewis acid sites is revealed for Ca-ZrPC, which correlates with the lowest density of hydroxyls (Broensted acid sites) bound with Zr cations (see Fig. 4, *a*).

Pt supporting was found to decrease absorption in the 3700–3720 cm^{-1} range, thus implying participation of a part of bridging hydroxyls in its fixation. The density of coordinatively unsaturated Zr cations probed by CO adsorbed at 77 K was decreased as well (spectra not shown for brevity). Hence, both types of acid sites located at zirconia pillars appear to take part in anchoring Pt clusters. Low-intensity carbonyl band at ~2125 cm^{-1} observed for oxygen-pretreated Pt-ZrPC samples indicates that Pt is mainly in the oxidized form possibly, due to strong interaction with nanosized pillars.

For copper-loaded pillared clays, in the carbonyl region, bands corresponding to both weak (stable only at 77 K) and strong (persisting evacuation at room temperature) CO complexes were observed. The position of those bands was independent upon the type of cation used

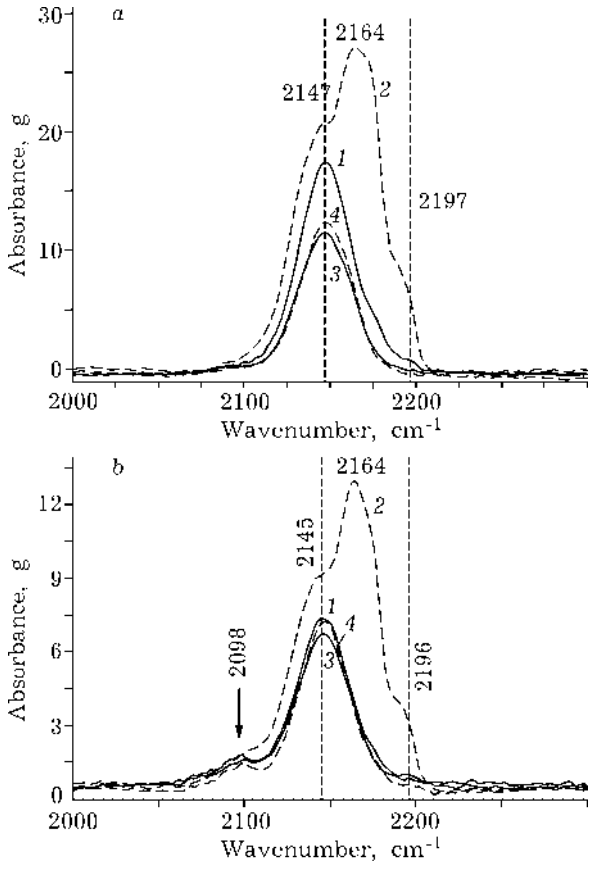

Fig. 5. FTIRS spectra of CO adsorbed at the surface of 1.4 % Cu/Ce-ZrPC (*a*) and spectra of CO adsorbed at the surface of 0.3 % Pt + 1.4 % Cu/Ce-ZrPC sample (*b*): *a* – PD-106, *b* – PD-118; *1* – 10 Torr CO, 290 K; *2* – 10 Torr CO, 77 K; *3* – CO chem., 290 K; *4* – CO chem., 77 K.

for the pillars modification, though intensity varied markedly. A detailed discussion of the effect of pillar stabilizing cation on the spectral features of CO adsorbed on copper-loaded samples is beyond the scope of this paper and will be presented elsewhere. Here, as a typical example, Fig. 5 illustrates the effect of Pt on the state of copper cations pre-fixed at zirconia pillars stabilized by cerium cations.

The most strong band at ~2160 cm^{-1} observed only at 120 K corresponds to CO complexes with hydroxyls [8] and will not be further discussed. The band at 2148 cm^{-1} stable to room temperature evacuation is due to Cu^{+}–CO complexes. This band position is independent upon the temperature of adsorption affecting its intensity. Hence, no coverage-dependent chemical or dynamic frequency shift is observed. This feature is typical for isolated (no identical neighbors in their vicinity) coordinatively unsaturated surface centers [8, 23]. Along with the high-frequency band position similar to that found earlier for isolated Cu^{+} cations incorporated into the surface layer of alumina support [23], this spectral feature allows to assign this band to CO adsorbed on Cu^{+} cations strongly bound with nanosized zirconia pillars. This suggests that those cations are coordinated by bridging oxygen atoms or hydroxyls bound simultaneously with highly charged Zr cations. Though some clustering of copper cations can be suggested by ESR and UV-Vis data (*vide supra*), FTIRS and EXAFS (*vide supra*) data agree the best with the model of very small (pares *etc.*) clusters comprised of the inaccessible cation(s) incorporated into the pillar, and only one of them is accessible to CO molecule.

In the spectrum recorded at room temperature in the presence of gas-phase CO, a shoulder at ~2175 cm^{-1} is clearly observed. Its intensity is much higher at 120 K under 10 Torr of CO, though its position remains nearly the same. This band can be assigned to Cu^{2+}–CO complexes [8]. Similar to the case of Cu^{+}–CO band (*vide supra*), at the level of copper loading used in those samples, this suggests that the surface Cu^{2+} cations have no identical neighbors in their vicinity. This conclusion agrees with the fact that for clustered copper cations supported on bulk partially stabilized zirconias or alumina, positions of bands corresponding to both Cu^{+}–CO (ν_{CO} ~ 2130–2115 cm^{-1}) and Cu^{2+}–CO ((ν_{CO} ~ 2185–2175 cm^{-1}) complexes is red-shifted with coverage [8].

Estimation of the number of Cu^{+} and Cu^{2+} cations by using known values of the integral absorption coefficients A_0 by Seanor and Amberg [28] revealed that around a half of copper cations is in the 1+ state. This share is much higher than that revealed for copper-loaded alumina [23] or bulk zirconia [8] samples, implying Cu^{+} cations stabilization by nanosized zirconia pillars.

Hence, three-dimensional reactive copper oxidic clusters dominating for copper supported bulk mesoporous zirconia catalysts [8] are absent for Cu-ZrPC samples. This feature can be assigned to difference between the surface arrangement of the most developed (111) and (110) faces of the fluorite-like zirconia and that

of nanosized zirconia pillars (*vide supra*). As the result, copper cations supported on nanosized pillars appear to sink into their bulk, thus being coordinated by bridging hydroxyls and/or oxygen atoms, reactive terminal oxygen forms being absent.

At room temperature, Pt atoms are detected by a Pt–CO band at ~2100 cm^{-1} (see Fig. 5, *b*), which is masked in spectrum recorded at low temperatures by a broad absorption corresponding to physically adsorbed CO. Since for Pt-ZrPC Pt is mainly in the ionic state due to strong interaction with pillars (*vide supra*), pre-supporting of copper cations appears to make such an interaction much weaker. Moreover, Pt supporting on sample precovered by copper cations causes two-three fold decrease of the intensity of bands corresponding to all types of other CO adsorption centers including Cu cations, Zr^{4+} cations and hydroxyls. Hence, a part of copper cations is masked by superimposed Pt atoms.

Temperature programmed reduction

The results for H_2 TPR for the initial ZrPC and samples of ZrPC loaded with Pt, Cu and Pt + Cu are presented in Fig. 6. For the initial pillared clay, temperature programmed reduction (TPR) peaks can be assigned to reduction of clustered (low temperatures) or isolated (high temperatures) admixed Fe cations.

In the case of Cu ZrPC, TPR maxima are shifted to much higher temperatures as compared with those for Cu-loaded bulk zirconia samples with even lower copper content (from *ca.* 200 °C [29] to *ca* 500 °C). This implies much stronger interaction of copper cations with nanosized zirconia particles and, hence, much higher oxygen bonding strength. This conclusion agrees well with the FTIRS data of adsorbed CO (*vide supra*).

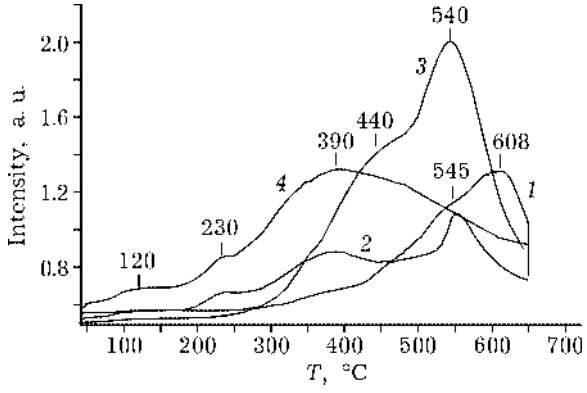

Fig. 6. H_2 TPR spectra for either pure Ca-ZrPC (*1*) or loaded with 0.3 % Pt (*2*), 1.4 % mass Cu (*3*), and 0.3 % Pt + 1.4 % mass Cu (*4*).

For Pt-containing sample, the hydrogen consumption starts at 100–200 °C with maxima at 230, 390 and 545 °C.

For Pt + Cu-containing sample, the TPR spectrum resembles that of Pt with the increased intensity of all peaks, while features corresponding to copper cations reduction are not observed. It implies (at least, a partial) shielding of copper cations by juxtaposed Pt clusters. The increase of the peaks intensity suggests strong interaction between supported Pt clusters and neighboring/underlying copper cations.

Temperature-programmed desorption of NO_x

For ZrPC as well as for Pt-supported ZrPC samples, two peaks of NO_x desorption are observed after room-temperature NO adsorption (not shown for brevity). The low-temperature peak comprised of NO molecules (T_{max} ~ 90 °C, desorbed <20 % of ad-NO_x) can be assigned to decomposition of nitrosyls located at coordinatively unsaturated Zr^{4+} cations. In the high-temperature part of TPD spectrum, an intense peak of evolved NO_2 (T_{max} ~ 360–380 °C) and a much smaller one of NO (T_{max} ~ 410 °C) are observed. Those peaks could be tentatively assigned to decomposition of nitrite species (yielding NO_2) and bridging nitrates (yielding NO) [30]. Pt supporting decreases the integral amount of adsorbed NO_x species (from 3.6 10^{18} to 2.6 10^{18} molecules/g), the first peak declining much stronger (3–4 times). This suggests that in both cases ad-NO_x species are mainly bound with coordinatively unsaturated Zr^{4+} cations, their density decreasing after Pt supporting.

For Cu-loaded PC, two peaks at ~120 and ~260 °C comprised nearly exclusively of NO_2 molecules are observed. Typical example is shown in Fig. 7 for copper supported on Ca-ZrPC. For other samples of Cu-loaded ZrPC studied here, the TPD peaks position remains

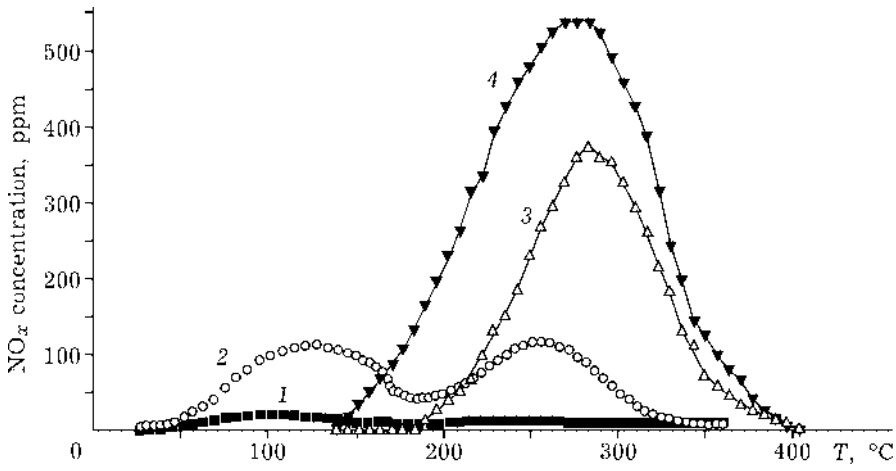

Fig. 7. TPD of NO_x for Ca-ZrPC-based samples loaded with 1.4 % mass Cu or 1.4 % mass CuO + 0.3 % mass Pt: *1* and *2* – CuO/ZrPC, NO and NO_x, respectively; *3* and *4* – Pt + CuO/ZrPC, NO and NO_x, respectively.

nearly identical, the integral amount of desorbed NO_x varying in the range of 0.5–2 10^{18} molecules/g. Hence, for copper-supported samples ad-NO_x adsorption centers are radically changed as compared with those of PC and can be assigned to copper cations. Such a type of NO_x TPD spectrum is completely different from that earlier observed for copper cations supported on partially stabilized zirconia [8] or alumina [30]. The main difference is that for the latter systems high-temperature (350–400 °C) peaks are comprised of NO molecules, thus being assigned to decomposition of bridging nitrates located on clusters of copper cations. This specificity of NO_x TPD spectrum for Cu-ZrPC agrees with conclusion on a higher degree of coordination saturation of copper cations fixed at the surface of nanosized pillars as compared with that in the case of copper cations on bulk zirconia supports (*vide supra*).

For Pt + Cu-loaded ZrPC (see Fig. 7), the TPD spectrum differs considerably from those coresponding to separate components and pure support. First of all, the integral amount of desorbed NO increases. Another important feature consists in the absence of the low-temperature peak corresponding to nitrosyls. Hence, either sites of nitrosyls adsorption are blocked, or during the temperature ramp, nitrosyls are decomposed or oxidized by weakly bound reactive oxygen. Moreover, the high-temperature peak is shifted to higher temperatures being now composed from nearly equal proportion of NO_2 and NO. As was shown by FTIRS of adsorbed CO (*vide supra*), the density of coordinatively unsaturated copper cations decreases due to Pt supporting. It implies that nitrate surface species generated due to Pt supporting are bound with both Pt atoms and copper cations. Earlier [11], by using *in situ* FTIRS, bridging nitrates were shown to be reactive intermediates in the NO_x propane SCR.

Catalytic activity

Propane. For ZrPC and Pt-supported ZrPC only deep oxidation of propane without NO_x reduction was observed (not shown for brevity). Hence, catalytic properties of ZrPC differ dramatically from those of bulk partially stabilized zirconias reasonably active in the high temperature range [9]. This difference appears to be explained by the different structural properties of nanosized pillars resulting in much lower density of Lewis acid sites (vide supra) responsible both for hydrocarbon activation and stabilization of reactive nitrate surface species [5, 7–9, 30]. The activity of Cu-supported samples is rather low even in the high-temperature range (typical results are presented in Fig. 8 for samples with pillars modified by alkaline-earth cations), being much worse than that of copper-loaded bulk zirconia samples (NO_x conversions up to 70 % were obtained at temperatures in the range of 350–400 °C [9, 10]). There is straightforward correlation between the poor performance of Cu/ZrPC samples and their low reducibility (*vide supra*).

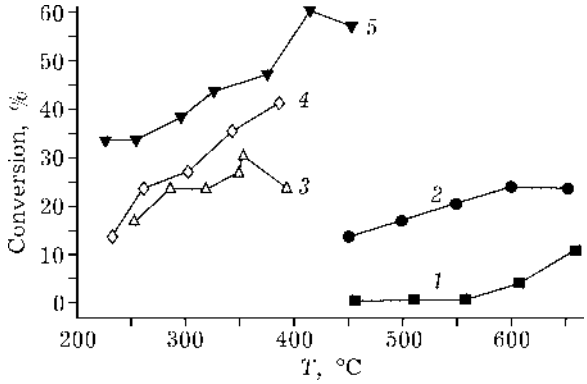

Fig. 8. Temperature dependence of NO_x conversion into N_2 in the propane SCR for ZrPC stabilized by alkaline-earth cations loaded with Cu or Pt + Cu: *1* –Cu/Ca-ZrPC, *2* – Cu/Sr-ZrPC, *3* – Pt, Cu/Ca-ZrPC, *4* – Pt, Cu/Sr-ZrPC, *5* – Pt, Cu/Ba-ZrPC.

Pt addition greatly improves performance and shifts it to the low-temperature range. The effect of Pt is explained by the increase of the active component oxidation ability (*vide supra*) ensuring a higher rate of propane activation, thus leading to its faster transformation along both routes –combustion and selective NO_x reduction (propane conversion *vs.* temperature not shown for brevity). For mixed active component, the SCR route is also apparently favored by the increase of the surface coverage by reactive nitrite-nitrate species due to Pt addition (*vide supra*).

Propylene. For the case of propylene as reductant, for ZrPC, very low (not exceeding 5–10 %) conversions of NO into nitrogen were observed, and propylene was mainly consumed by the deep oxidation route. Here, performance of nanosized zirconia particles drastically differs with that of bulk zirconia samples, which are highly active and selective in propylene NO_x SCR [31].

ZrPC loaded with a small (0.1–0.2 % mass) amount of Pt was moderately active in the propylene SCR with a maximum degree of NO_x conversion not exceeding 40 % at 300 °C, nitrous oxide selectivity being around 10 %. Detailed results on catalytic properties of Pt-loaded ZrPC in propylene NO_x SCR will be presented elsewhere.

Catalytic properties of zirconia-pillared clays loaded with copper cations are demonstrated in Fig. 9. In the case of pillars modified by Ce and Fe cations, the maximum level of NO_x conversion does not exceed 40 %. When pillares are modified by alkaline-earth cations, the maximum conversion is somewhat higher (up to 60 %, the results for those samples are not shown for brevity). Apparently higher efficiency of NO_x reduction by propylene as compared with propane, especially at lower temperatures, is rather general trend, which is usually explained by more facile activation of the former reductant [9]. At temperatures lower T_{max} of NO conversion, rates of NO reduction appear to correlate with those of propylene con-

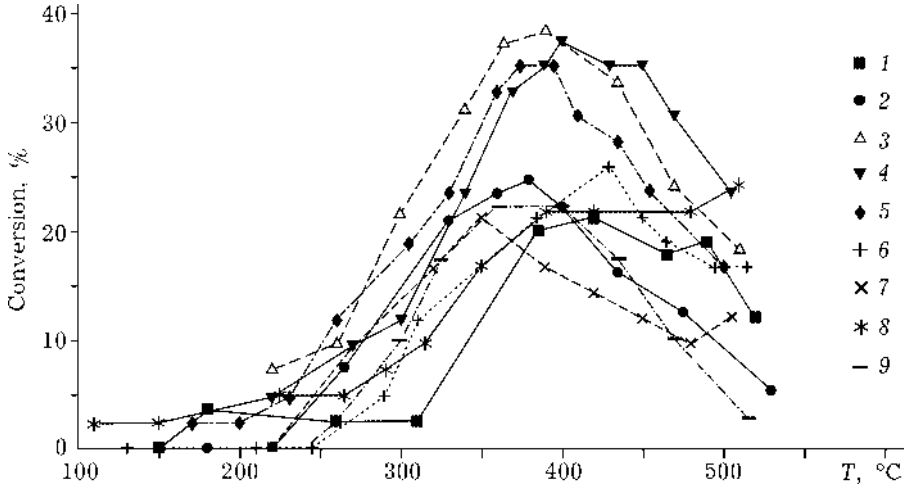

Fig. 9. Temperature dependence of conversions of NO_x in propylene SCR for 1.4 % mass CuO supported PCs with pillars modified by Ce and Fe (% mass): 0.02 Ce (*1*), 0.06 Ce (*2*), 0.36 Ce (*3*), 0.6 Fe (*4*), 0.76 Fe (*5*), 0.6 Fe (*6*), 1.1 Fe (*7*), 0.08 Ce (*8*), 1.0 Fe (*9*); clays contain 20 % ZrO_2 (*1*–*8*), 15 % ZrO_2 (*9*) with pillaring carried out at 60 °C (*1*–*7*) or 25 °C (*8* and *9*); copper content 1.4 % mass.

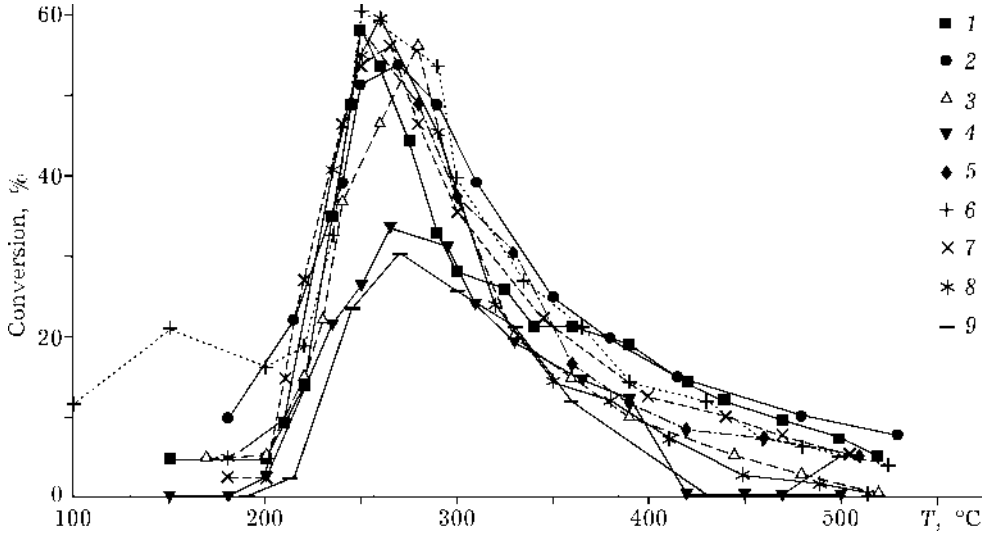

Fig. 10. Temperature dependence of conversions of NO_x in propylene SCR for Pt + Cu supported PCs modified by Ce and Fe cations. Curves designation is the same as in Fig. 9.

sumption [9], which suggests importance of propylene activation for NO_x SCR. However, another factors such as carbonaceous deposits accumulation or C,N-intermediates transformation could be of importance as well [9].

Modification of Cu-ZrPC samples by Pt shifts the range of efficient performance to lower temperatures and increases the maximum value of NO_x conversion to 60 % for pillars stabilized by Ce or Fe cations (Fig. 10) or to 80 % for samples with pillars stabilized by alkaline-earth cations. This effect apparently correlates with the increase of the rate of propylene consumption (not shown here for brevity). In all cases, N_2O selectivity was <10 %, and the features of the reaction mechanism explaining this behavior contrasting with a high nitrous oxide selectivity for alumina-supported Pt [32] will be presented elsewhere.

Decane. In the case of decane as reductant, copper-loaded samples with alumina – or zirconia pillars either pure or stabilized by alkaline-earth cations were found to be inactive in the NO_x SCR. In contrary, for pillars modified by Ce or Fe cations, some copper-loaded samples demonstrate a good performance in the NO_x selective reduction by decane (Fig. 11). No nitrous oxide was observed among products in

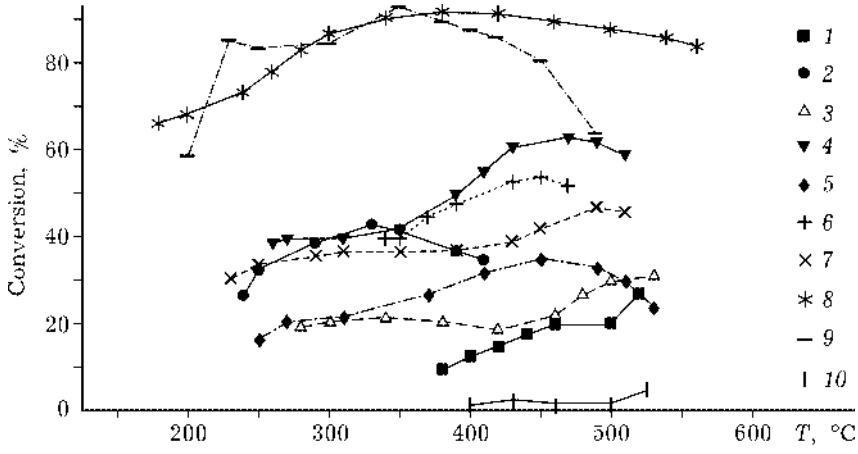

Fig. 11. Temperature dependence of NO_x conversion in decane SCR for Cu supported PCs modified by Ce and Fe (% mass): 0.02 Ce (*1*), 0.06 Ce (*2*), 0.36 Ce (*3*), 0.6 Fe (*4*), 0.76 Fe (*5*), 0.6 Fe (*6*), 1.09 Fe (*7*), 0.08 Ce (*8*), 0.31 Ce (*9*), 1.0 Fe (*10*); clays contain 20 % ZrO_2 (*1–8*), ~15 % ZrO_2 (*9* and *10*) with pillaring carried out at 60 °C (*1–7*) or 25 °C (*8–10*); copper content 1.4 % mass.

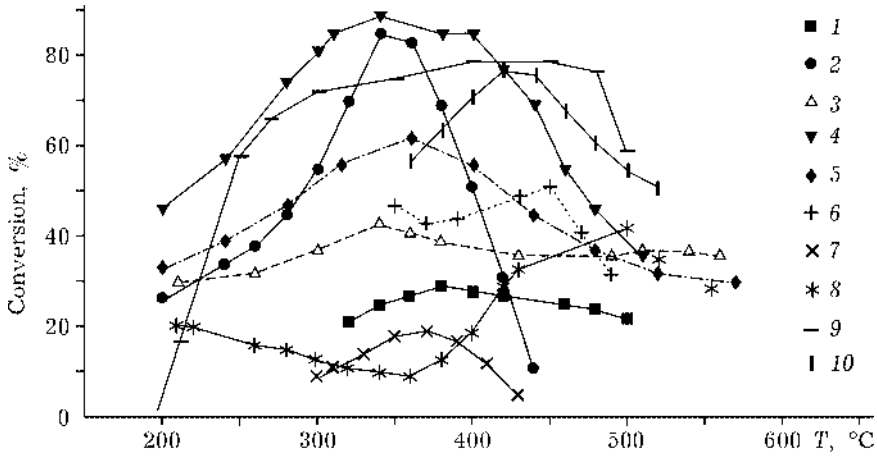

Fig. 12. Temperature dependence of NO_x conversion in decane SCR for Pt-Cu supported PCs, modified by Ce and Fe cations. Curves designation is the same as in Fig. 11.

those experiments in mixtures with a high oxygen content (20 %) for both series of Cu- or Pt + Cu-loaded ZrPC samples.

Since Ce or Fe cations could help to increase the combustion ability of the active component thus decreasing coking, this factor is probably responsible for the increase of performance. Indeed, the highest level of NO_x conversion was observed for samples with pillars modified by Ce cations (see Fig. 11). This conclusion agrees with pronounced coking of ZrPC-based samples (after reaction, samples are black due to coke deposition), which leads to their deactivation through plugging of micropores when mixtures of NO and decane contain relatively low (though excess) amount of oxygen (1–2 %). Nevertheless, the absence of any strict dependence between the nature or content of stabilizing cation and activity suggests a strong effect of the spatial distribution/size of pillars as well. Indeed, when the pillaring was carried out for 16–20 h at 60 °C, the performance was lower for Ce-containing samples (curves *1–3*) as compared with those containing Fe (curves *4–7*). When pillaring was carried out at room temperature for 24–48 h, hence, less uniform spatial distribution of pillars is expected [14], the highest activity in a broad temperature range was observed for samples containing Ce cations apparently less favoring coking (curves *8, 9*). More detailed analysis of the pillars spatial distribution on samples performance in decane SCR is beyond the scope of this paper and will be presented elsewhere. A high level of NO_x conversion at temperatures as low as 200 °C for some systems appears to be very promising for practice.

In the case of Pt-promoted samples, a general level of activity is enhanced, though a broad scattering of NO_x conversion values remains and the operation temperature range is somewhat narrowed (Fig. 12). Again, improvement of performance by Pt addition can be explained by enhanced oxidation ability of mixed active components. A high performance level was observed for Pt + Cu-loaded samples with pillars stabilized either by Ce, Fe or Ca cations. The best performance (see Fig. 12) is obtained for sample N4 with a lower (15 %) content of pillar modified by Fe which implies the importance of diffusion limitations.

Performance of best Cu + Pt/ZrPC samples in decane NO_x SCR in the low-temperature range exceeds that of such systems as Cu + Ag/zirconia [9], copper/sulfated zirconia [33], copper/mordenite [34] or copper-exchanged b-zeolite [35], which makes them interesting for the practical application.

CONCLUSIONS

Procedures for synthesis of Cu + Pt loaded montmorillonite clays pillared with zirconia nanoparticles stabilized by alkaline earth, Ce and Fe cations were elaborated, and their textural, structural and surface properties were elucidated by using a variety of techniques.

These systems with combined metal-oxide active components were found to possess a good performance in the NO_x selective reduction by propane, propylene and decane in the excess of oxygen. The specificity of the catalytic action of these systems stems from pronounced interaction between the active components and nanosized zirconia pillars as well as between active components. For the reaction of NO_x reduction by long-chain hydrocarbon – decane, the details of the pore structure appear to be of a great importance both due to diffusion limitations and/or coking able to block the interlayer space. Combination of low- and high-temperature catalysts based upon ZrPC and bulk mesoporous zirconia supports within a unified catalytic layer could be promising for broadening the operation temperature range.

Acknowledgement

This work is in part supported by INTAS 97–11720 project.

REFERENCES

1 M. Iwamoto, *Stud. Surf. Sci. Catal.,* 130 (2000) 23.
2 A. Shichi, K. Katagi, A. Satsuma and T. Hattori, *Appl. Catal.*, B. 24 (2000) 97.
3 R. T. Yang, N. Tharappiwattananon and R. Q. Long, *Ibid.*, B 19 (1998) 289.
4 F. Figueras, *Catal. Rev.-Sci. Eng.*, 30 (1988) 457.
5 G. A. Konin, A. N. Il'ichev, V. A. Matyshak *et al.*, *Topics in Catal.*, 17 (2001) 193.
6 V. A. Sadykov, T. G. Kuznetsova, V. P. Doronin *et al.*, *Mat. Res. Soc. Proc. Ser.,* 703 (2002) V 13.21.
7 V. A. Sadykov, R. V. Bunina, G. M. Alikina *et al.*, Nanophase and Nanocomposite Materials III, in S. Komarneni, H. Hahn and J. Parker (Eds.), Mater. Res. Soc. Proc. Ser., Warrendale, PA, 2000, vol. 581, p. 435.
8 V. A. Sadykov, R. V. Bunina, G. M. Alikina *et al.*, *J. Catal.,* 200 (2001) 117.
9 V. A. Sadykov, R. V. Bunina, G. M. Alikina *et al.*, *Ibid.*, 200 (2001) 131.
10 O. V. Metelkina, V. V. Lunin, V. A. Sadykov *et al., Ibid.*, 78 (2002) 111.
11 V. A. Sadykov, E. A Paukshtis, S. A. Beloshapkin *et al., J. Environ. Studies*, 1 (1997) 21.
12 J. H. de Boer, B. J. Linsen and R. H. Osinga, *J. Catal.*, 4 (1965) 643.
13 M. M. Dubinin, *Carbon*, 23 (1985) 373.
14 A. Gil and L. M. Gandia, *Catal. Rev.-Sci. Eng.*, 42 (2000) 145.
15 L. M. Gandia, M. A. Vicente and A. Gil, *Appl. Catal. A: General,* 196 (2000) 281.
16 P. Canizares, J. L. Valverde, M. R. Sun Kou and C. V. Molina, *Micropor. Mesop. Mat.*, 29 (1999) 267.
17 H. Auer and H. Hofmann, *Appl. Catal. A: General*, 97 (1993) 23.
18 M. L. Occelli, A. A Auroux and G. I. Ray, *Micropor. Mesop. Mat.*, 39 (2000) 43.
19 M. L. Occelli, J. A. Bertand, S. A. C. Gould and J. M. Dominguez, *Ibid.*, 34 (2000) 195.
20 K. Ohtsuka, Y. Hayashi and M. Suda, *Chem. Mater.*, 5(1993) 1823.
21 M. Aberg, *Acta Chem. Scand., Ser. A*, 31 (1977) 172.
22 V. F. Anufrienko, N. G. Maximov, V. G. Shinkarenko *et al.*, Application of Zeolites in Catalysis, Nauka, Novosibirsk, 1977, p. 129 (in Russian).
23 S. F. Tikhov, V. A. Sadykov, G. N. Kryukova *et al., J. Catal.,* 134 (1992) 506.
24 A. Martinez-Arias, R. Cataluna, J. C. Conesa and J. Soria, *J. Phys. Chem. B.,* 102 (1998) 809.
25 A. A. Tsyganenko, V. N. Filimonov, *Uspekhi fotoniki,* 4 (1974) 51.
26 A. N. Kharlanov, N. A. Zubareva, E. V. Lunina *et al., Vestn. MGU, Ser. 2. Khimiya,* 39 (1998) 29.
27 V. Indovina, M. Occhiuzzi, D. Pietrogiacomi and S. Tuti, *J. Phys. Chem.*, 103 (1999) 9967.
28 D. A. Seanor and G. H. Amberg, *J. Chem. Phys.*, 42 (1970) 2907.
29 M. Shimokawabe, H. Asakawa and N. Takezawa, *Appl. Catal.*, 59 (1990) 45.
30 V. A. Sadykov, S. L. Baron, V. A. Matyshak *et al., Catal. Lett.*, 37 (1996) 157.
31 G. A. Konin, A. N. Il'ichev, V. A. Matyshak *et al.*, The Mechanism of NO_x SCR by Propylene in the Excess of O_2 on ZrO_2, Europacat-V, September, Abstracts, 2001, Book 2, 21–O–10.
32 R. Burch, P. Fornasiero and B. W. L. Southward, *J. Catal.,* 182 (1999) 234.
33 G. Delahay, E. Ensuque, B. Coq and F. J. Figueras, *Ibid.,* 175 (1998) 7.
34 B. Coq, D. Tachon and F. Figueras, *Catal. Lett.*, 35 (1995) 183.
35 G. Delahay, B. Coq and L. Broussous, *Appl. Catal. B,* 12 (1997) 49.